In Situ Radiometric and Exposure Age Dating of the Martian Surface

K. A. Farley,[1]* C. Malespin,[2] P. Mahaffy,[2] J. P. Grotzinger,[1] P. M. Vasconcelos,[3] R. E. Milliken,[4] M. Malin,[5] K. S. Edgett,[5] A. A. Pavlov,[2] J. A. Hurowitz,[6] J. A. Grant,[7] H. B. Miller,[1] R. Arvidson,[8] L. Beegle,[9] F. Calef,[9] P. G. Conrad,[2] W. E. Dietrich,[10] J. Eigenbrode,[2] R. Gellert,[11] S. Gupta,[12] V. Hamilton,[13] D. M. Hassler,[13] K.W. Lewis,[14] S. M. McLennan,[6] D. Ming,[15] R. Navarro-González,[16] S. P. Schwenzer,[17] A. Steele,[18] E. M. Stolper,[1] D. Y. Sumner,[19] D. Vaniman,[20] A. Vasavada,[9] K. Williford,[9] R. F. Wimmer-Schweingruber,[21] the MSL Science Team†

We determined radiogenic and cosmogenic noble gases in a mudstone on the floor of Gale Crater. A K-Ar age of 4.21 ± 0.35 billion years represents a mixture of detrital and authigenic components and confirms the expected antiquity of rocks comprising the crater rim. Cosmic-ray–produced ^{3}He, ^{21}Ne, and ^{36}Ar yield concordant surface exposure ages of 78 ± 30 million years. Surface exposure occurred mainly in the present geomorphic setting rather than during primary erosion and transport. Our observations are consistent with mudstone deposition shortly after the Gale impact or possibly in a later event of rapid erosion and deposition. The mudstone remained buried until recent exposure by wind-driven scarp retreat. Sedimentary rocks exposed by this mechanism may thus offer the best potential for organic biomarker preservation against destruction by cosmic radiation.

Multiple orbiter and rover missions have documented a rich geologic record on the surface of Mars, likely spanning almost the entire history of the planet [e.g., (*1*)]. However, interpretation of this record is impeded by our limited understanding of the connection between the materials observed and their absolute age. Impact crater densities are the primary means for establishing a chronology for geologic features on Mars and other solar system bodies (*2*–*4*), but crater-based dating methods suffer from multiple sources of uncertainty that obscure both absolute and relative ages. In contrast, on Earth, isotopic dating methods provide a powerful quantitative framework for defining geologic history and for identifying the rates and causes of geologic phenomena. Here, we report results of an attempt to apply in situ isotopic dating methods to Mars using the instrument suite aboard the Curiosity rover exploring Gale Crater.

Geologic Setting

Gale is a ~150-km diameter impact crater that formed near the Late Noachian–Early Hesperian boundary (*5*, *6*) or around 3.7 to 3.5 billion years ago (Ga) according to impact crater models (*3*, *7*). In addition to the ~5-km-high central mountain of stratified rock informally known as Mt. Sharp, the crater is partially filled with sedimentary rocks derived from the crater rim. Crater-density distributions imply a somewhat younger age (Early to Late Hesperian or ~3.5 to 2.9 Ga) for at least some of these deposits (*5*, *6*). While heading for its destination at Mt. Sharp, Curiosity traversed a gently sloping plain where local outcrops of pebble conglomerate were encountered, recording the presence of an ancient stream bed (*8*). Most of this surface is heavily cratered and covered with rock and soil (Fig. 1). However, a substantial expanse of bare bedrock was encountered in an ~5-m-deep topographic trough (Yellowknife Bay) representing an erosional window through a sequence of stratified rocks known as the Yellowknife Bay formation (fig. S1) (*9*). These rocks consist mostly of distal alluvial fan and lacustrine facies of basaltic bulk composition and were derived from the crater rim (*9*, *10*). Compared with adjacent geological units, the Yellowknife Bay trough is notable for its lack of visible craters and its apparently greater degree of stripping of impact ejecta and wind-blown soil. This appearance suggests active erosion, distinctly different from the adjacent map units (*9*). However, the depositional age of the Yellowknife Bay formation, its stratigraphic relationship to the adjacent alluvial fan and to the strata of Mt. Sharp, and the causes and timing of its exposure are all presently uncertain.

As shown in Fig. 1, the Sheepbed mudstone and stratigraphically overlying Gillespie Lake sandstone of the Yellowknife Bay formation (*9*) form a rock couplet of apparently variable rock hardness, and their contact has eroded to form a decimeter-scale topographic step. The Sheepbed–Gillespie Lake contact is sharp and marked by scouring of the underlying mudstone, producing a small scarp and in some locations an overhang. Calved-off blocks of the sandstone occur at the base and a few meters outboard of the scarp but not beyond [see figure 3 of (*9*)]. This suggests that residual fragments of the degrading scarp are removed efficiently enough to leave only a very thin lag deposit at locations where the Gillespie Lake member is now completely absent.

The distinctive erosional profile of the Sheepbed–Gillespie Lake contact can be traced around the full width of Yellowknife Bay (*9*), with the Sheepbed unit making up the floor of the encircled trough. This trough is elongated in the northeast-southwest direction, creating an amphitheater-shaped planimetric form open to the northeast. Beyond the Gillespie Lake contact, the more-resistant units higher in the section form similar scarps stepping upward a total of ~5 m to the uppermost unit of the Yellowknife Bay formation (fig. S1). Within the Sheepbed unit, mm- to cm-scale topographic protrusions form fields of small ridges that have been streamlined in the northeast-southwest direction (Fig. 2). Along with the morphology of the Yellowknife Bay trough, these features indicate a dominant role for southwest-directed wind erosion. These observations implicate eolian processes in eroding the mudstone, in efficiently wearing down any blocks that are delivered to its surface from the encircling scarps or from distal impacts, and in expanding the exposure of the Yellowknife Bay formation.

Scientific investigations at Yellowknife Bay focused on the Sheepbed mudstone. This fine-grained (<50 μm) rock was drilled twice for mineralogical and evolved gas analyses (*11*, *12*). In addition, multiple chemical analyses were obtained on outcropping mudstone as well as the drill tailings. The two drilled samples, referred to as John Klein and Cumberland, were located ~3 m apart and yielded very similar results. The mudstone is composed of detrital and authigenic components consisting of both crystalline and x-ray amorphous phases (*11*).

[1]Division of Geological and Planetary Sciences, California Institute of Technology, Pasadena, CA 91125, USA. [2]NASA Goddard Space Flight Center, Greenbelt, MD 20771, USA. [3]School of Earth Sciences, University of Queensland, Brisbane, Queensland QLD 4072, Australia. [4]Department of Geological Sciences, Brown University, Providence, RI 02912, USA. [5]Malin Space Science Systems, San Diego, CA 92121, USA. [6]Department of Geosciences, Stony Brook University, Stony Brook, NY 11794, USA. [7]Center for Earth and Planetary Studies, National Air and Space Museum, Smithsonian Institution, 6th at Independence SW, Washington, DC 20560, USA. [8]Department of Earth and Planetary Sciences, Washington University in St. Louis, St. Louis, MO 63130, USA. [9]Jet Propulsion Laboratory, California Institute of Technology, Pasadena, CA 91109, USA. [10]Earth and Planetary Science Department, University of California, Berkeley, CA 94720, USA. [11]Department of Physics, University of Guelph, Guelph, ON N1G 2W1, Canada. [12]Department of Earth Science and Engineering, Imperial College London, London SW7 2AZ, UK. [13]Southwest Research Institute, Boulder, CO 80302, USA. [14]Department of Geosciences, Princeton University, Princeton, NJ 08544, USA. [15]NASA Johnson Space Center, Houston, TX 77058, USA. [16]Instituto de Ciencias Nucleares, Universidad Nacional Autónoma de Mexico, Ciudad Universitaria, México D.F. 04510, Mexico. [17]Department of Physical Sciences, CEPSAR, Walton Hall, Milton Keynes MK7 6AA, UK. [18]Carnegie Institution, Geophysical Laboratory, Washington, DC 20015, USA. [19]Department of Geology, University of California, Davis, CA 95616, USA. [20]Planetary Science Institute, Tucson, AZ 85719, USA. [21]University of Kiel, Kiel D-24098, Germany.

*Corresponding author. E-mail: farley@gps.caltech.edu

†MSL Science Team authors and affiliations are listed in the supplementary materials.

The detrital fraction includes minerals typical of volcanic rocks: plagioclase; pyroxenes; and minor olivine, sanidine, and ilmenite. Crystalline authigenic phases include smectitic clay (possibly saponite) and magnetite, thought to have formed as a result of chemical alteration of detrital olivine, and minor akaganeite, pyrrhotite, bassanite, and hematite. Quartz and halite were reported but very near the Chemistry and Mineralogy instrument (CheMin) detection limit. Chlorate or perchlorate was also tentatively identified (*12*). A model for the amorphous component, comprising about one-third of the sample, indicates that it is composed mainly of Si, Fe, Ca, S, and Cl (*11*). It likely includes poorly crystalline or finely crystalline materials and may include detrital volcanic and impact-derived glass. The presence of smectite, magnetite, and akaganeite suggests that the mudstone has not experienced burial heating above ~200°C (*11*, *13*). It is possible that the sample experienced no burial heating at all.

Geochronology Overview: K/Ar and Cosmogenic Isotopes

Noble gas isotopes can quantitatively constrain the age and erosion history of the Sheepbed mudstone. Argon-40 from ^{40}K decay decay will record a potassium-weighted average of the formation or cooling ages of the multiple components of the mudstone. Isotopes ^{36}Ar, ^{21}Ne, and ^{3}He are produced by irradiation of the uppermost ~2 to 3 m of the martian surface by galactic cosmic rays (GCRs) (*14*). These cosmogenic isotopes are commonly used to assess exposure histories of meteorites [e.g., (*15*, *16*)] and erosion rates and styles of terrestrial rocks [e.g., (*17*)]. Because the martian atmosphere is very thin and the magnetic field very weak (*18*), the martian surface is only weakly shielded from GCRs. Thus cosmogenic isotope-production rates are much higher than on Earth (*14*, *19*). The chemistry of the Sheepbed mudstone (*10*) is such that the most abundant cosmogenic isotope is likely to be ^{36}Ar produced from the capture of cosmogenic thermal neutrons by Cl; followed by ^{3}He produced by spallation mainly of O, Si, and Mg; followed by ^{21}Ne from spallation of Mg, Si, and Al (*20*). The mudstone's exposure history is thus recorded by multiple isotopic systems.

The depth dependence of the production functions of the two spallation isotopes are very similar: a small maximum at ~15 cm below the surface, reflecting development of the nuclear cascade in the uppermost layers of rock, followed by an exponential decay over 2 to 3 m as the energetic particles attenuate (Fig. 3). In contrast, the production rate of ^{36}Ar from neutron capture has a larger subsurface maximum at greater depth (~60 cm), arising from the combined effects of the production of neutrons within the descending cascade and the loss of low-energy neutrons into the martian atmosphere [e.g., (*19*)].

The concentration of a single cosmogenic isotope yields a nonunique exposure history for the rock. The customary end-member interpretive models are to assume either no erosion, in which case a surface exposure age is obtained, or steady erosion from great depth, in which case a mean erosion rate is obtained [e.g., (*17*)]. Figure 3 shows that this nonuniqueness can be eliminated by combining spallogenic and neutron-capture isotope measurements. In particular, a rock of Sheepbed composition initially at a depth of greater than a few meters that was instantaneously exposed at the surface would have $^{36}Ar/^{3}He$ of ~1.5 and $^{36}Ar/^{21}Ne$ of ~13. In contrast, if steady erosion causes progressive downward migration of the surface toward the sample, then the sample integrates the entire depth profile, including the large subsurface ^{36}Ar peak. Such a rock would have $^{36}Ar/^{3}He$ ~ 4 and $^{36}Ar/^{21}Ne$ ~ 30. In both erosion scenarios, the $^{3}He/^{21}Ne$ ratio is ~8; this isotope pair provides a cross-check but no additional information on exposure history.

Results and Discussion

Geochronology measurements were performed on the Cumberland drilled powder (*21*). After

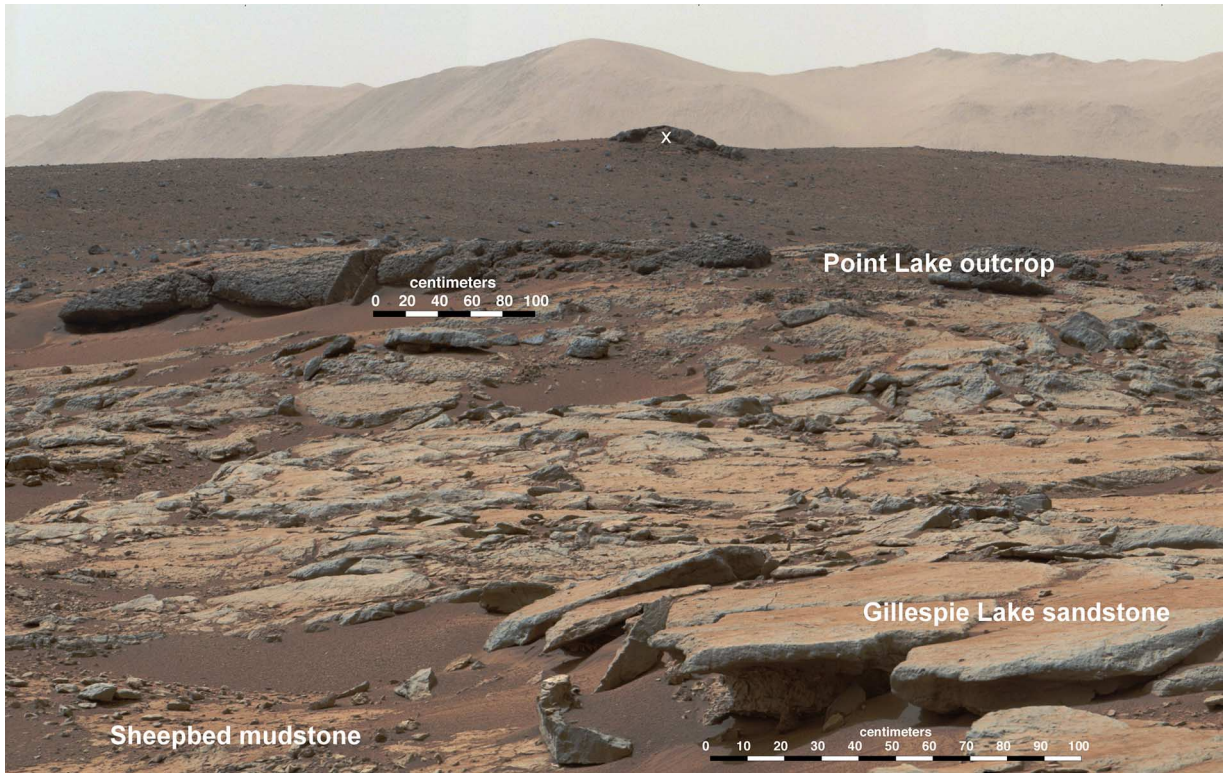

Fig. 1. Mastcam view looking 79° west of north. With increasing distance, the Yellowknife Bay formation includes the Sheepbed mudstone, Gillespie Lake sandstone, and Point Lake outcrop (36 m away). In the distance, the mostly rock- and sand-covered Bradbury rise is visible. The large outcrop on the near horizon (marked "x") is 240 m distant and stands 13 m above the Gillespie Lake–Sheepbed contact. This is a portion of a 40-frame M-100 mosaic taken on sol 188 between 13:27 and 13:48 local mean solar time (14 February 2013 23:41:35 and 15 February 2013 00:03:23 Pacific Standard Time). The images in the full mosaic, acquired as sequence mcam01009, have picture identifications between 0188MR0010090000202415I01 and 0188MR0010090390202454I01.

drilling, the sample was sieved, and an aliquot with estimated mass of 135 ± 18 mg (*22*) was introduced into a quartz cup in the Sample Analysis at Mars (SAM) instrument. The cup was moved into position in an oven, sealed against Mars atmosphere, and evacuated. The sample was then heated to a maximum temperature of ~890°C for 25 min, and the evolved gases were purified and admitted into the quadrupole mass spectrometer for analysis. All reported measurements used the high-sensitivity semistatic analysis mode.

K-Ar Age

The Ar concentration and the Alpha Particle X-ray Spectrometer (APXS)–determined K_2O concentration yield a K-Ar age of 4.21 ± 0.35 Ga (1σ) for the Cumberland sample (Table 1). This age calculation assumes that all measured ^{40}Ar is radiogenic (*23*). Although a fairly uniform level of excess Ar is thought to be present in some young martian meteorites (*24*), that same level of excess would contribute <0.03 billion years to the age of this high K_2O, high Ar concentration rock. One important implication of this very high K-Ar age is that processing in the SAM oven has extracted essentially all radiogenic ^{40}Ar despite a fairly low extraction temperature. This unexpectedly high yield (*25*) may result from rapid diffusive loss from the inherently fine grain size of the mudstone [probably enhanced by the powdering process of the drill (*26*)]. Alternatively, the volatile constituents in the mudstone may promote loss via flux-induced melting. Because fine grain size and flux melting will affect the noble gas isotopes similarly, effective extraction of ^{36}Ar, ^{21}Ne, and ^{3}He might also be expected. The high age also implies that a very large fraction of the radiogenic Ar was retained in the mudstone over geologic time.

The interpretation of the K-Ar age depends critically on where potassium is located in the rock. If a fraction F_D of the potassium is in the detrital phases and the remainder in authigenic phases, then the bulk age (T_B) is a potassium-weighted average of the age of the detritus (T_D) and the age of authigenesis (T_A): $T_B = (1 - F_D) T_A + F_D T_D$. If all of the potassium is carried in the detrital components (mainly sanidine, plagioclase, and possibly basalt glass), $F_D = 1$. In this case, the K-Ar system records a mixture of the ages of components present in the crater rim, principally bedrock ranging from minimally to completely reset by the Gale-forming impact. Crater-rim lithologies, as well as the crater itself, are thought to range from Noachian to Early Hesperian in age or about 4.1 to 3.5 Ga (*5*, *6*, *27*–*29*), in agreement with the K-Ar age of 4.21 ± 0.35 Ga that we measured. Because formation of K-bearing authigenic phases can only lower the mudstone age below that of the detrital component, we conclude with 95% confidence (*30*) that the potassium-weighted mean age of the materials in the Gale crater wall exceeds 3.6 Ga. Alternatively, if the potassium is entirely hosted within authigenic components (phyllosilicates or amorphous phases other than basalt glass), $F_D = 0$ and the age records the formation age of those phases. In this case, 4.21 Ga would represent a minimum age of mudstone deposition.

At present, we have no definitive way to determine the potassium distribution in the mudstone, but we can make a reasonable estimate. K-bearing phases determined by CheMin include sanidine (1.8%), andesine feldspar (21%), and an unknown fraction of basaltic or impact glass (*11*). CheMin cannot determine the K_2O content of any of these phases, so we assume representative values of 13%, 0.3%, and 1%, respectively (*31*). By assuming the mudstone

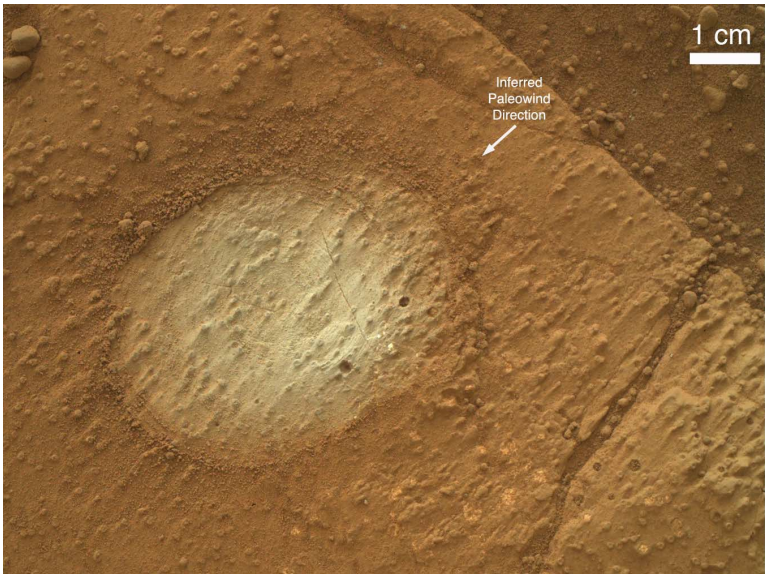

Fig. 2. Mars Hand Lens Imager (MAHLI) image of brushed, gray bedrock outcrop of Sheepbed mudstone near the Cumberland drill hole. Protrusion of nodules (*9*) results from eolian scouring of rock surface, creating wind tails. Preference for steep faces of wind tails on northeast side suggests a long-term averaged paleowind direction from northeast to southwest. This is a portion of MAHLI image 0291MH0001970010103390C00, acquired on sol 291. Illumination from the upper left.

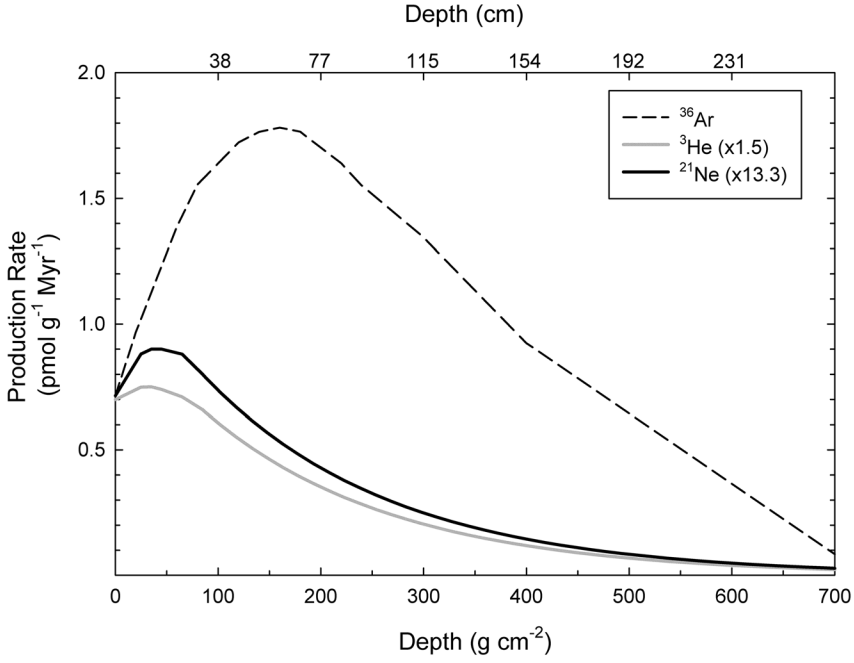

Fig. 3. Depth dependence of cosmogenic isotope-production rates modeled for a rock of Cumberland mudstone chemistry on Mars. Helium-3 and ^{21}Ne are spallation isotopes, whereas ^{36}Ar is produced by capture of cosmogenic neutrons. Note the multiplicative factors applied to ^{3}He and ^{21}Ne. A mudstone bulk density of 2.6 g cm^{-3} was assumed to convert overburden mass to linear depth.

contains 10% glass, we conclude that the detrital component accounts for 80% of the measured K_2O. The remainder could then be in the authigenic clay (18% of the mudstone) with 0.6% K_2O, in agreement with K_2O concentrations in saponite in a martian meteorite (*32*). If we assume $T_D < 4.1$ Ga on the basis of crater-count ages of the Gale impact and host terrains and use the 95% confidence lower limit on the K-Ar age of 3.6 Ga, we obtain a current best estimate that the mudstone was deposited before 1.6 Ga. Assuming either a younger age for the detrital component or a smaller fraction of it in the mudstone would cause this estimate to rise.

Cosmogenic ^{36}Ar, ^{21}Ne, and ^{3}He

Isotopes ^{36}Ar, ^{21}Ne, and ^{3}He were all detected at levels that cannot be attributed to sources other than cosmic ray irradiation (*33*). In the mudstone, ^{36}Ar/^{3}He and ^{36}Ar/^{21}Ne are 1.7 ± 0.5 and 12 ± 5, respectively (*34*). These ratios are within error of predictions of the no-erosion scenario (1.5 and 13) and very different from the prediction of the steady-erosion scenario (4 and 30). Thus, we cast our results in terms of surface-exposure age, which for ^{3}He, ^{21}Ne, and ^{36}Ar are 72 ± 15, 84 ± 28, and 79 ± 24 Ma, respectively. These ages could be the sum of multiple shorter exposure intervals separated by burial events, for example, by exposure during initial deposition and then again by recent reexposure or alternatively by burial and exhumation associated with migrating eolian deposits. However, these events would have to involve rapid burial and removal of at least a few meters of cover to maintain the good match of measured nuclide concentration ratios to those of production at the surface.

The agreement among these results argues for complete extraction of all three noble gases in the SAM oven and against substantial loss of noble gases over the ~78-million-year (My) period of cosmic ray exposure. For example, diffusive loss of He from amorphous phases, plagioclase, and phyllosilicates might occur at Mars ambient temperature (*35*), but the ^{3}He/^{21}Ne ratio of ~7.5 ± 2.6 matches the expected production ratio of ~8. Similarly, dissolution and reprecipitation of a water-soluble Cl-rich phase by occasional wetting of the mudstone might release accumulated ^{36}Ar. If this occurred to a substantial extent, then the agreement between the ^{36}Ar exposure age and the ^{21}Ne and ^{3}He exposure ages would have to be fortuitous. Although not impossible, we see no evidence for it in these data.

A substantial portion of the ^{3}He and ^{21}Ne must be carried by detrital minerals, including plagioclase and pyroxene, because these are important host phases for the major target elements (*36*). In contrast, the enrichment of Cl compared with a typical martian basalt suggests that much of this element was added to the mudstone from solution (*9*, *10*). This distinction implies that, although ^{3}He and ^{21}Ne might record cosmic-ray irradiation that occurred during primary exposure and transport in addition to that acquired during modern exposure at Yellowknife Bay, the same is not true of ^{36}Ar. The logical interpretation of the good agreement among all three exposure ages is that all three reflect exposure only in the modern setting.

The apparent absence of a detrital cosmogenic signal favors deposition of the mudstone in an environment in which erosion and transport were fairly rapid and/or in which the martian surface was shielded from cosmic rays by a reasonably dense atmosphere. The transition from comparatively wet conditions and a thick atmosphere to cold and dry conditions with a thin atmosphere is thought to have occurred around the Noachian-Hesperian boundary (*37*). Because wet conditions favor rapid erosion, in either scenario the cosmogenic isotope observations would support deposition of the Sheepbed mudstone shortly after Gale formation. Alternatively, deposition may have occurred in association with a later event in which material was eroded and transported rapidly enough to prevent detectable cosmogenic production. A late erosional event has also been suggested for Amazonian-age fan formation in some other martian craters (*38*–*40*).

Topography, stratigraphy, and surface-exposure dating suggest that the Yellowknife Bay trough is currently a focus of erosion and that erosion is occurring by scarp retreat. The Sheepbed mudstone lies below a sequence of relatively more-resistant units that define a series of topographic steps (A to A′ in fig. S1). The pace of wind erosion for the entire escarpment will be set by the retreat rate of these more-resistant units. However, deflation of the softer units, such as the mudstone, undercuts and contributes to collapse of the resistant layers (Fig. 1), such that both direct wind abrasion of resistant units and removal of the softer units contribute to slope retreat. Resistant units and corresponding local steps will thicken or thin as erosion sweeps into units with variable thicknesses and resistance properties. This predominately lateral erosion has caused scarp migration to the southwest and possibly other directions and produced several meters of surface lowering. The general flattening of the topographic profile (fig. S1) as it extends into the Yellowknife Bay trough may indicate that a more-resistant unit beneath the Sheepbed mudstone has slowed continued removal of this unit.

In such a model, the scarp retreat rate can be estimated from the surface-exposure ages. To prevent cosmogenic nuclide accumulation requires at least 2 to 3 m of overburden. Southwestward from the drill site (and downwind, according to Fig. 3), this amount of overburden is first encountered about 60 m away (fig. S1). Thus, in a model in which the mudstone is rapidly exposed from >2- to 3-m depth to the surface, the scarp retreat rate over the last ~80 My averages ~0.75 m My^{-1}. At this rate, the full extent of the Yellowknife Bay exposure could have been produced over several hundred million years of steady lateral erosion. Alternatively, wind erosion and associated scarp retreat may be highly episodic, perhaps in response to climatic variations tied to Mars' obliquity cycle (*41*, *42*). Either way, surface-exposure ages may vary substantially around the Yellowknife Bay outcrop and other similar exposures, in principle offering a test of the scarp retreat hypothesis.

Table 1. Geochronology data. The elemental composition was obtained from APXS measurement of Cumberland drill tailings from Sheepbed mudstone. PR is the model isotope production rate (*47*). Surface exposure age assuming no erosion. Indicated uncertainty is one standard deviation.

Cumberland sample mass		**0.135 ± 0.018 g**				
		K-Ar system				
K_2O (wt %)	0.50	±0.08				
^{40}Ar (nmol/g)	11.95	±1.71				
K-Ar Age (Ga)	4.21	±0.35				
		Cosmogenic isotopes				
			PR (pmol g^{-1} Ma^{-1})		Exposure age	
Isotope	pmol/g	±	Surface	2-m average	(Ma)	±
^{3}He	33.7	6.9	0.466	0.171	72	15
^{21}Ne	4.49	1.52	0.054	0.025	84	28
^{36}Ar	55.6	16.8	0.714	1.029	78	24

Implications for Organic Preservation

Cosmic rays penetrating the uppermost several meters of rock create a cascade of atomic and subatomic particles, electrons, and photons that ionize molecules and atoms in their path [e.g., (*43*, *44*)]. Complex organic molecules are particularly susceptible to degradation by such particles, and, because these particles also produce the cosmogenic nuclides, we have a way to assess the likely magnitude of this degradation in the Cumberland sample. Degradation of organic molecules in martian surface rocks subjected to cosmic-ray irradiation has been modeled (*44*). When scaled to the long-term cosmic-ray dose implied by the cosmogenic nuclides in the Cumberland sample, these rates predict reductions of between 2 and 3 orders of magni-

tude in the concentration of organic molecules in the 100– to 400–atomic mass unit range.

The scarp retreat hypothesis offers a possible strategy for minimizing the degree of organic degradation in samples obtained during the further course of exploration by Curiosity and possible future missions. Because exposure ages and thus cosmic-ray doses should decrease toward a bounding scarp (at least in the downwind direction), such a location may offer the best potential for organic preservation. Given our estimated scarp retreat rate, locations within a few tens of cm of a few-meter-scale scarp may have been exposed to cosmic rays for less than a few My. Such a short exposure compares favorably to what can reasonably be expected from alternative sampling strategies relying on recent impact craters or drilling to obtain fresh strata.

References and Notes

1. M. H. Carr, J. W. Head III, Geologic history of Mars. *Earth Planet. Sci. Lett.* **294**, 185–203 (2010). doi: 10.1016/j.epsl.2009.06.042
2. E. M. Shoemaker, R. J. Hackman, R. E. Eggleton, "Interplanetary correlation of geologic time," in *Advances in the Astronautical Sciences* (Plenum, New York, 1962), vol. 8, pp. 70–89.
3. W. K. Hartmann, G. Neukum, Cratering chronology and the evolution of Mars. *Space Sci. Rev.* **96**, 165–194 (2001). doi: 10.1023/A:1011945222010
4. W. K. Hartmann, Martian cratering 8: Isochron refinement and the chronology of Mars. *Icarus* **174**, 294–320 (2005). doi: 10.1016/j.icarus.2004.11.023
5. L. Le Deit *et al.*, Sequence of infilling events in Gale crater, Mars: Results from morphology, stratigraphy, and mineralogy. *J. Geophys. Res. Planets* n/a (2013). doi: 10.1002/2012JE004322
6. B. J. Thomson *et al.*, Constraints on the origin and evolution of the layered mound in Gale Crater, Mars using Mars Reconnaissance Orbiter data. *Icarus* **214**, 413–432 (2011). doi: 10.1016/j.icarus.2011.05.002
7. B. A. Ivanov, Mars/Moon cratering rate ratio estimates. *Space Sci. Rev.* **96**, 87–104 (2001). doi: 10.1023/A:1011941121102
8. R. M. E. Williams *et al.*, Martian fluvial conglomerates at Gale crater. *Science* **340**, 1068–1072 (2013). doi: 10.1126/science.1237317; pmid: 23723230
9. J. P. Grotzinger *et al.*, A habitable fluvio-lacustrine environment at Yellowknife Bay, Gale crater, Mars. *Science* **343**, 1242777 (2014); doi: 10.1126/science.1242777
10. S. M. McLennan *et al.*, Elemental geochemistry of sedimentary rocks at Yellowknife Bay, Gale crater, Mars. *Science* **343**, 1244734 (2014); doi: 10.1126/science.1244734
11. D. Vaniman *et al.*, Mineralogy of a mudstone at Yellowknife Bay, Gale crater, Mars. *Science* **343**, 1243480 (2014); doi: 10.1126/science.1243480
12. D. W. Ming *et al.*, Volatile and organic compositions of sedimentary rocks in Yellowknife Bay, Gale crater, Mars. *Science* **343**, 1245267 (2014); doi: 10.1126/science.1245267
13. L. P. Keller *et al.*, Aqueous alteration of the Bali CV3 chondrite: Evidence from mineralogy, mineral chemistry, and oxygen isotopic compositions. *Geochim. Cosmochim. Acta* **58**, 5589–5598 (1994). doi: 10.1016/0016-7037(94)90252-6; pmid: 11539152
14. D. Lal, Cosmogenic and nucleogenic isotopic changes in Mars: Their rates and implications to the evolutionary history of Martian surface. *Geochim. Cosmochim. Acta* **57**, 4627–4637 (1993). doi: 10.1016/0016-7037(93)90188-3; pmid: 11539580
15. O. Eugster, Cosmic-ray exposure ages of meteorites and lunar rocks and their significance. *Chem. Erde-Geochem.* **63**, 3–30 (2003). doi: 10.1078/0009-2819-00021
16. K. Marti, T. Graf, Cosmic-ray exposure history of ordinary chondrites. *Annu. Rev. Earth Planet. Sci.* **20**, 221–243 (1992). doi: 10.1146/annurev.ea.20.050192.001253
17. T. Cerling, H. Craig, Geomorphology and in-situ cosmogenic isotopes. *Annu. Rev. Earth Planet. Sci.* **22**, 273–317 (1994). doi: 10.1146/annurev.ea.22.050194.001421
18. M. H. Acuña *et al.*, Magnetic field and plasma observations at Mars: Initial results of the Mars Global Surveyor mission. *Science* **279**, 1676–1680 (1998). doi: 10.1126/science.279.5357.1676; pmid: 9497279
19. M. N. Rao, D. D. Bogard, L. E. Nyquist, D. S. McKay, J. Masarik, Neutron capture isotopes in the martian regolith and implications for Martian atmospheric noble gases. *Icarus* **156**, 352–372 (2002). doi: 10.1006/icar.2001.6809
20. Cosmogenic production-rate calculations are given in the supplementary materials.
21. Full method details are provided in the supplementary materials.
22. Details of mass estimate and uncertainty are given in the supplementary materials.
23. Atmospheric and excess argon are assumed negligible, as described in the supplementary materials.
24. D. Bogard, J. Park, D. Garrison, ^{39}Ar-^{40}Ar "ages" and origin of excess ^{40}Ar in Martian shergottites. *Meteorit. Planet. Sci.* **44**, 905–923 (2009). doi: 10.1111/j.1945-5100.2009.tb00777.x
25. Full release of Ar for Ar geochronology often requires much higher temperatures. See supplementary materials for a discussion of this issue.
26. R. C. Anderson *et al.*, Collecting samples in Gale Crater, Mars; an overview of the Mars Science Laboratory sample acquisition, sample processing and handling system. *Space Sci. Rev.* **170**, 57–75 (2012). doi: 10.1007/s11214-012-9898-9
27. D. H. Scott, M. G. Chapman, Geologic and topographic maps of the Elysium paleolake basin, Mars. *U.S. Geol. Surv. Misc. Invest. Map I-2397* (1995).
28. R. Greeley, J. E. Guest, Geologic map of the eastern equatorial region of Mars. *U.S. Geol. Surv. Misc. Invest. Map I-1802-B* (1987).
29. J. J. Wray, Gale crater: the Mars Science Laboratory/Curiosity rover landing site. *Int. J. Astrobiol.* **12**, 25–38 (2013). doi: 10.1017/S1473550412000328
30. We used the cumlative normal distribution.
31. Potassium concentrations were estimated from terrestrial examples of volcanic sanidine and andesine [e.g., (*45*, *46*)]. The relatively high K_2O content assumed for the basalt glass is consistent with ongoing analyses of basalts in Gale Crater. The K_2O concentration and glass abundance can be traded off to yield the same overall mass balance.
32. J. C. Bridges, S. P. Schwenzer, The nakhlite hydrothermal brine on Mars. *Earth Planet. Sci. Lett.* **359-360**, 117–123 (2012). doi: 10.1016/j.epsl.2012.09.044
33. Possible alternative sources and why they can be neglected are described in the supplementary materials.
34. Mass errors cancel in these ratios.
35. Laboratory data bearing on the question of diffusive noble gas loss are given in the supplementary materials.
36. Likely host minerals for each of the noble gases are given in the supplementary materials.
37. J.-P. Bibring *et al.*, Global mineralogical and aqueous Mars history derived from OMEGA/Mars Express data. *Science* **312**, 400–404 (2006). doi: 10.1126/science.1122659; pmid: 16627738
38. J. A. Grant, S. A. Wilson, Late alluvial fan formation in southern Margaritifer Terra, Mars. *Geophys. Res. Lett.* **38**, L08201 (2011). doi: 10.1029/2011GL046844
39. J. A. Grant, S. A. Wilson, A possible synoptic source of water for alluvial fan formation in southern Margaritifer Terra, Mars. *Planet. Space Sci.* **72**, 44–52 (2012). doi: 10.1016/j.pss.2012.05.020
40. N. Mangold *et al.*, The origin and timing of fluvial activity at Eberswalde crater, Mars. *Icarus* **220**, 530–551 (2012). doi: 10.1016/j.icarus.2012.05.026
41. J. Laskar *et al.*, Long term evolution and chaotic diffusion of the insolation quantities of Mars. *Icarus* **170**, 343–364 (2004). doi: 10.1016/j.icarus.2004.04.005
42. W. R. Ward, Large-scale variations in the obliquity of Mars. *Science* **181**, 260–262 (1973). doi: 10.1126/science.181.4096.260; pmid: 17730940
43. L. R. Dartnell, L. Desorgher, J. M. Ward, A. J. Coates, Modelling the surface and subsurface Martian radiation environment: Implications for astrobiology. *Geophys. Res. Lett.* **34**, L02207 (2007). doi: 10.1029/2006GL027494
44. A. A. Pavlov, G. Vasilyev, V. M. Ostryakov, A. K. Pavlov, P. Mahaffy, Degradation of the organic molecules in the shallow subsurface of Mars due to irradiation by cosmic rays. *Geophys. Res. Lett.* **39**, L13202 (2012). doi: 10.1029/2012GL052166
45. W. A. Deer, R. A. Howie, J. Zussman, *Framework Silicates - Feldspars*, vol. 4A of *Rock-Forming Minerals* (Geological Society of London, London, 2001).
46. O. Bachmann, M. A. Dungan, P. W. Lipman, The Fish Canyon magma body, San Juan volcanic field, Colorado: Rejuvenation and eruption of an upper-crustal batholith. *J. Petrol.* **43**, 1469–1503 (2002). doi: 10.1093/petrology/43.8.1469
47. Calculations are provided in supplementary materials.

Acknowledgments: The authors are indebted to the Mars Science Laboratory (MSL) Project engineering and management teams for their exceptionally skilled and diligent efforts in making the mission as effective as possible and enhancing science operations. We are also grateful to all those MSL team members who participated in tactical and strategic operations. Without the support of both the engineering and science teams, the data presented here could not have been collected. Three anonymous reviewers provided many helpful suggestions. Some of this research was carried out at the Jet Propulsion Laboratory, California Institute of Technology, under a contract with the National Aeronautics and Space Administration. Data presented in this paper are archived in the Planetary Data System (pds.nasa.gov).

Supplementary Materials

www.sciencemag.org/content/343/6169/1247166/suppl/DC1
Materials and Methods
Figs. S1 to S3
Tables S1 to S4
References (*48*–*67*)

14 October 2013; accepted 25 November 2013
Published online 9 December 2013;
10.1126/science.1247166